Ocean Dynamics (2011) 61:543–558
DOI 10.1007/s10236-011-0381-z

Analytical solution for the tidally induced Lagrangian residual current in a narrow bay

Wensheng Jiang · Shizuo Feng

Received: 2 October 2010 / Accepted: 13 January 2011 / Published online: 29 January 2011

Abstract In a weakly nonlinear tidal system, the depth-averaged equations for the first-order Lagrangian residual velocity (LRV) are deduced systematically. For the case of a narrow bay, the equations are solved analytically and the results for a specific bottom profile are discussed in detail. According to the pattern of the first-order LRV, the bay can be divided into three parts, namely an inner part, a transitional zone, and an outer part. For the given depth profile, the streamline of the first-order LRV for a shorter bay is a part of that for a longer bay. The first-order LRV depends on a nondimensional parameter that combines the influences of the bottom friction coefficient, the tidal period and the averaged water depth. The form of the bottom friction also has a significant influence on the first-order LRV. The second-order LRV, i.e., the Lagrangian drift, is analytically solved and shows dependence on the initial tidal phase. The LRV differs from the Eulerian residual transport velocity both quantitatively and qualitatively. It is demonstrated that the residual currents obtained according to other definitions may cause misunderstanding of the mass transport in water exchange applications.

Responsible Editor: Richard John Greatbatch

W. Jiang (✉) · S. Feng
Physical Oceanography Laboratory,
Ocean University of China, Songling Road 100, Qingdao,
Shandong, 266100, People's Republic of China
e-mail: wsjang@ouc.edu.cn

S. Feng
e-mail: szfeng@ouc.edu.cn

Keywords Lagrangian residual current · Eulerian residual velocity · Eulerian residual transport velocity · Analytical solution · Weakly nonlinear tidal system · Narrow bay

1 Introduction

In shallow seas, the tidal current is normally the dominant component of the total movement of the sea water. Because of nonlinearity, the tidal flow induces an aperiodic current that is called the residual current. It has been long recognized that the residual current plays an important role in the inter-tidal mass transport in the shallow seas (e.g., Nihoul and Ronday 1975).

The meaning of "residual current" is rather vague, which is related to the various ways to derive it from the directly measured current fields. The residual current and the accompanying temperature and salinity fields should constitute a slowly varying, aperiodic dynamic system in shallow seas. The prerequisite for the retrieved aperiodic movement to become the residual current is that it can describe the net displacement of the water parcel after one or a few tidal periods. The residual current should also be in accordance with the basic law of fluid motion.

A straightforward definition of the residual current is the average of the measured velocity at a fixed location over multiple tidal periods (e.g., Abbott 1960). This is called the Eulerian residual velocity, $\mathbf{u_E}$. However, if $\mathbf{u_E}$ is used to study the inter-tidal movement in a 3D case, there is fictitious source (or sink) of water mass at the sea surface (Feng et al. 1984). There is also an extra-dispersion term in the inter-tidal transport

equation (Fischer et al. 1979). These are questionable aspects related to describing the subtidal current with the Eulerian residual velocity.

An alternative approach to define the residual velocity was inspired by the idea of relating the mass-transport velocity to the sediment transport in tidal estuaries by Hunt (1961). Longuet-Higgins (1969) first related the mass-transport velocity to the large-scale ocean circulation. He pointed out clearly that the mass-transport velocity at a fixed location is not solely controlled by the mean velocity at that point alone, and the mass-transport velocity, $\mathbf{u_L}$, equals the sum of the Eulerian residual velocity ($\mathbf{u_E}$) and the Stokes' drift velocity ($\mathbf{u_S}$). For the case of the tidal flow, Zimmerman (1979) obtained the analytic expression of $\mathbf{u_S}$ and found that $\mathbf{u_L}$ and $\mathbf{u_E}$ are rather different; Loder (1980) and Cheng and Casulli (1982) demonstrated similar results based on numerical modeling results.

In a weakly nonlinear tidal system, Feng et al. (1986a) systematically applied the perturbation method to the depth-averaged tidal dynamic equations and obtained the Lagrangian residual velocity (LRV, hereafter), $\mathbf{u_{LR}}$, to the second order expressed by the zeroth-order tidal solutions. They showed that the first-order $\mathbf{u_{LR}}$ is the mass-transport velocity, $\mathbf{u_L}$; and defined the second-order $\mathbf{u_{LR}}$ as the Lagrangian drift velocity, $\mathbf{u_{ld}}$. They analytically revealed the dependence of $\mathbf{u_{ld}}$ on the tidal phase, which is related to the initial timing when the water parcels are released. This demonstrates that $\mathbf{u_{LR}}$ has a specific Lagrangian nature (Cheng 1983). Feng et al. (1986b) proposed the use of $\mathbf{u_L}$ to replace $\mathbf{u_E}$ to act as the advective transport velocity in the inter-tidal transport equation, in which the tidal dispersion term disappears.

Feng (1987) extended the analysis to the 3D case and established a set of dynamic equations governing $\mathbf{u_L}$. A tidal body force appears in the momentum equations, which represents the nonlinear coupling of the zeroth-order tide. The water mass is continuous at the sea surface, i.e., the fictitious "tidal surface source" in Feng et al. (1984) vanishes, which keeps the conservation of the mass. The inter-tidal mass-transport equation using $\mathbf{u_L}$ as the advective velocity was also derived, with the tidal dispersion term in Fischer et al. (1979) disappearing. The analysis clearly demonstrated that $\mathbf{u_L}$ is the more appropriate residual circulation in the tide-dominant shallow seas.

The distinction between the Lagrangian and the Eulerian residual velocity has been theoretically recognized for more than 30 years. The Lagrangian residual current framework has been successfully applied to many cases (e.g., Jay 1991; Foreman et al. 1992; Dortch et al. 1992; Cerco and Cole 1993; Wang et al. 1993; Ridderinkhof and Loder 1994; Delhez 1996; Wei et al. 2004; Hainbucher et al. 2004; Muller et al. 2009). However, the Lagrangian framework is still not widely accepted; and it is not uncommon in literature that the Eulerian residual velocity ($\mathbf{u_E}$) is used to explain the mass transport in shallow seas. This is partly because the residual current is at least one order smaller than the tidal current, causing it to be often contaminated by the errors in observations or model simulations. This leads to difficulty in demonstrating the differences among various definitions of the residual current.

In some special cases, $\mathbf{u_E}$ was questioned explicitly based on the physics. For example, when studying the depth-averaged 2D case, Robinson (1983) replaced $\mathbf{u_E}$ with the Eulerian residual transport velocity, $\mathbf{u_T}$, as the tidal mean flux at one specific location divided by the averaged water depth. He stated that $\mathbf{u_T}$ should be used to quantify the mean mass transport at a specific location. This statement was proven wrong by Feng et al. (1986b) who showed it is $\mathbf{u_L}$ rather than $\mathbf{u_T}$ that is related to the inter-tidal transport. The product of the depth-averaged LRV and the mean water depth, the so-called Lagrangian residual transport, is the net mass transport in a depth-averaged 2D case. Since $\mathbf{u_T}$ is of the same order as $\mathbf{u_E}$ and $\mathbf{u_L}$, it is also difficult to distinguish them from observations or modeling results.

Under such a circumstance, the analytical solutions for idealized cases are the most ideal for assessing the differences among different residual velocities. For example, Dyke (1980) gave an analytical solution of the Stokes' drift in a two-layer rectangular basin with a flat bottom, based on a specific solution of the linear tide. Ianniello (1977) analytically calculated $\mathbf{u_E}$ and $\mathbf{u_L}$ in a length-depth section of a narrow bay, and found that $\mathbf{u_E}$ is always seaward while $\mathbf{u_L}$ is of a two-layer structure. This clearly demonstrated that the Eulerian residual velocity violates mass conservation while the LRV does not. It should be pointed out that the expression of $\mathbf{u_L}$ in Ianniello (1977) is indeed $\mathbf{u_T}$, later defined by Robinson (1983). It happens that in the case of Ianniello (1977) $\mathbf{u_T}$ is a valid simplification of $\mathbf{u_L}$.

For general cases $\mathbf{u_T}$ and $\mathbf{u_L}$ are different, but in recent years $\mathbf{u_T}$ has still been used to represent the inter-tidal mass transport even in some theoretical studies. Li and O'Donnell (2005) gave an analytic solution of $\mathbf{u_T}$ in a narrow bay and used it to represent the mass-transport velocity. They studied the dependence of the Eulerian residual transport velocity on the length (Li and O'Donnell 2005) and bending of the bay (Li et al. 2008). Winant (2007) found a solution for a 3D case in a bay and then studied the first-order LRV, $\mathbf{u_L}$ (Winant 2008). However, he used the Eulerian residual transport to represent the depth integrated residual

transport even though he noticed the discrepancy between $\mathbf{u_T}$ and $\mathbf{u_L}$ in his results.

The purpose of the present study is to clarify the different definitions of the residual current, through quantitative comparison of $\mathbf{u_E}$, $\mathbf{u_T}$ and $\mathbf{u_L}$ calculated for a specific case of a narrow bay. The governing equations for the Lagrangian residual flow in a depth-averaged 2D case will be derived for the first time, based on the concept developed by Feng et al. (1986a,b). By confining to a narrow bay, the equations will be solved analytically to obtain the first- and second-order LRV. The behavior of the LRV will be analyzed and some factors influencing it will be discussed. The analysis results will help to draw the attention of researchers when studying the circulation dynamics in shallow coastal waters.

2 Definitions and governing equations

2.1 Definitions of residual velocities

For clarity, Table 1 provides a list of symbols related to the major definitions of the residual currents. The definitions of these residual currents are provided below, and more details can be found in Feng et al. (1986a, 2008) and Delhez (1996).

The Lagrangian residual velocity $\mathbf{u_{LR}}$ is commonly defined as the net displacement of the water parcel divided by the elapsed time of n tidal periods (e.g., Zimmerman 1979):

$$\mathbf{u_{LR}} = \frac{\boldsymbol{\xi}(t_0 + nT; \mathbf{x_0}, t_0)}{nT},$$

where $\boldsymbol{\xi}(t; \mathbf{x_0}, t_0) = \int_{t_0}^{t} \mathbf{u}(\mathbf{x_0} + \boldsymbol{\xi}, t')\mathrm{d}t'$ defines the displacement of a water parcel with the initial position at $\mathbf{x_0}$ when $t = t_0$.

The tidal oscillation is removed from the net displacement of the water parcel after n tidal periods, but a slowly varying part with an inter-tidal time scale τ may still exist. Feng et al. (2008) proved that if n is not too large to ensure that the water parcel's net displacement after n tidal periods is at least one order of magnitude smaller than the tidal excursion, $\boldsymbol{\xi}(t_0 + nT; \mathbf{x}_0, t_0)$ can be a smooth function of $\mathbf{x}_0$ and τ. Thus, assuming $\boldsymbol{\xi_{nr}}(\mathbf{x}_0, \tau; t_0) = \boldsymbol{\xi}(t_0 + nT; \mathbf{x}_0, t_0)$, the LRV is defined as

$$\mathbf{u_{LR}}(\mathbf{x_0}, \tau; t_0) = \frac{\partial \boldsymbol{\xi_{nr}}(\mathbf{x}_0, \tau; t_0)}{\partial \tau}$$

The nonlinearity of the shallow sea tidal system can be quantified by a nondimensional number κ, the ratio between the tidal amplitude and the water depth. In the weakly nonlinear case, i.e., $O(\kappa) < 1$, all the state variables such as u, υ and ζ can be expanded into the power series according to κ,

$$u = u_0 + \kappa u_1 + \kappa^2 u_2 + \cdots$$

and similar expansion can be applied to υ and ζ.

Feng et al. (1986a) proved that the mass-transport velocity $\mathbf{u_L}$ defined by Longuet-Higgins (1969) is the first-order approximation to $\mathbf{u_{LR}}$ and is independent of the initial phase t_0, i.e.,

$$\mathbf{u_{LR}}(\mathbf{x_0}, \tau; t_0) = \mathbf{u_L}(\mathbf{x_0}, \tau) + O(\kappa), \tag{1}$$

where the mass-transport velocity is defined as

$$\mathbf{u_L}(\mathbf{x_0}, \tau) = \mathbf{u_E} + \mathbf{u_S}. \tag{2}$$

The Eulerian residual velocity is defined as

$$\mathbf{u_E} = (u_E, \upsilon_E) = (\langle u_1 \rangle, \langle \upsilon_1 \rangle), \tag{3}$$

and the Stokes' drift velocity is defined as

$$\mathbf{u_S} = (u_S, \upsilon_S) = \langle \boldsymbol{\xi_0} \cdot \nabla \mathbf{u_0} \rangle, \tag{4}$$

where the tidal average operator is defined as follows:

$$\langle f \rangle = \frac{1}{nT} \int_{t_0}^{t_0 + nT} f(\mathbf{x}, t)\mathrm{d}t, \tag{5}$$

and

$$\boldsymbol{\xi_0} = (\xi_0, \eta_0) = \left(\int_{t_0}^{t} u_0(\mathbf{x}_0, t')\mathrm{d}t', \int_{t_0}^{t} \upsilon_0(\mathbf{x}_0, t')\mathrm{d}t' \right).$$

Thus,

$$\mathbf{u_0} = (u_0, \upsilon_0) = \frac{\partial \boldsymbol{\xi}_0}{\partial t}. \tag{6}$$

Table 1 Symbols for major definitions of the residual current

Symbol	Meaning
$\mathbf{u_{LR}}$	Lagrangian residual velocity(LRV)
$\mathbf{u_L}$	First-order LRV, mass-transport velocity
$\mathbf{u_{ld}}$	Second-order LRV, Lagrangian drift velocity
$\mathbf{u_E}$	Eulerian residual velocity
$\mathbf{u_S}$	Stokes' drift velocity
$\mathbf{u_T}$	Eulerian residual transport velocity

The definition of the Eulerian residual transport velocity $\mathbf{u_T}$ is based on the idea that the calculation of the residual transport should take the water surface oscillation into consideration, thus,

$$\mathbf{u_T} = (u_T, v_T) = \mathbf{u_E} + \frac{\langle \mathbf{u_0}\zeta_0 \rangle}{h}. \tag{7}$$

It is proved in Eqs. 53 and 54 in the Appendix (or Feng et al. 1986b) that

$$\mathbf{u_S} = \mathbf{u_D} + \frac{\langle \mathbf{u_0}\zeta_0 \rangle}{h},$$

where

$$\mathbf{u_D} = (u_D, v_D) = \frac{1}{h}\left(\frac{\partial \langle h u_0 \eta_0 \rangle}{\partial y}, \frac{\partial \langle h v_0 \xi_0 \rangle}{\partial x}\right). \tag{8}$$

We thus get $\mathbf{u_L} = \mathbf{u_T} + \mathbf{u_D}$, which means that $\mathbf{u_T}$ is only a part of $\mathbf{u_L}$. In general, even to the first-order approximation, $\mathbf{u_T}$ cannot describe the water parcel movement as the LRV does, except in cases when $\mathbf{u_D} = 0$ such as the section-averaged one-dimensional or breadth-averaged two-dimensional cases of a bay.

The second-order $\mathbf{u_{LR}}$ is related to the Lagrangian drift velocity $\mathbf{u_{ld}} = (u_{ld}, v_{ld})$,

$$\mathbf{u_{LR}} = \mathbf{u_L} + \mathbf{u_{ld}} + O(\kappa^2). \tag{9}$$

$\mathbf{u_{ld}}$ is dependent on the initial phase of a tidal period and its expression can be found in Feng et al. (1986a). The Lagrangian drift velocity represents the interaction between the tidal current and $\mathbf{u_L}$ and is one order smaller than $\mathbf{u_L}$ in the weakly nonlinear case.

2.2 The tidal equations

For a narrow bay, the Cartesian coordinates are used with the x and y-axes oriented along and across the axis of the bay respectively. The bay has a length of L and width of B. A single-frequency tide is imposed at the open boundary at $x = 0$. The nondimensional, depth-averaged governing equations describing this system of long gravity waves can be found in literature, e.g., in Feng et al. (1986a). Here we use the linearized quadric bottom friction based on Proudman (1953). The influence of the nonlinear bottom friction on the tide-induced residual current will be discussed in Section 4.4. The governing equations are

$$\frac{\partial \zeta}{\partial t} + \frac{\partial (h+\kappa\zeta)u}{\partial x} + \frac{\partial (h+\kappa\zeta)v}{\partial y} = 0, \tag{10}$$

$$\frac{\partial u}{\partial t} + \kappa\left(u\frac{\partial u}{\partial x} + v\frac{\partial u}{\partial y}\right) - \delta F v = -\frac{\partial \zeta}{\partial x} - \beta_T \frac{u}{h+\kappa\zeta}, \tag{11}$$

$$\delta^2\left[\frac{\partial v}{\partial t} + \kappa\left(u\frac{\partial v}{\partial x} + v\frac{\partial v}{\partial y}\right)\right] + \delta F u = -\frac{\partial \zeta}{\partial y} - \delta^2 \beta_T \frac{v}{h+\kappa\zeta}, \tag{12}$$

where t, $\mathbf{u} = (u, v)$, ζ and h are the nondimensional time, velocity and its components in x and y directions, sea surface elevation and water depth, respectively. For brevity, they take the same form as the dimensional variables.

The characteristic scales for the various variables are $t_c = T$, $x_c = \lambda$, $y_c = B$, $u_c = \sqrt{g/h_c}\zeta_c$ and $v_c = B\zeta_c/(h_c T)$, where h_c is the averaged water depth, ζ_c is the typical tidal amplitude at the open boundary, g is the acceleration due to gravity, and $\lambda = T\sqrt{gh_c}$ is the wave length.

Equations 10–12 contain four nondimensional parameters, i.e., $\kappa = \zeta_c/h_c$, $\delta = B/\lambda$, $F = fT$ and $\beta_T = \beta T/h_c$, where β is the bottom friction coefficient and f is the Coriolis parameter. The present study considers the semi-diurnal or diurnal tides and the bay is assumed to be located at the mid-latitude, so $O(F) = 1$. For tides in the shallow seas, the bottom friction is significant and should be included in the lowest-order tide equations, hence $O(\beta_T) = 1$. The third parameter κ, the ratio of the tidal amplitude over the water depth, characterizes the nonlinear effect in the system. The fourth parameter δ is the aspect ratio of the cross and along-channel length scales.

In this study, we consider the case of $O(\kappa) < 1$ and assume δ to be of the same order as κ, i.e., $O(\delta) = O(\kappa)$. This describes a system of weakly nonlinear tide in a narrow bay. The perturbation method can be applied to Eqs. 10–12 based on the small parameter κ.

Substituting the expansion of the state variables according to κ into Eqs. 10–12 yields the zeroth-order equations

$$\frac{\partial \zeta_0}{\partial t} + \frac{\partial h u_0}{\partial x} + \frac{\partial h v_0}{\partial y} = 0, \tag{13}$$

$$\frac{\partial u_0}{\partial t} = -\frac{\partial \zeta_0}{\partial x} - \beta_T \frac{u_0}{h}, \tag{14}$$

$$0 = \frac{\partial \zeta_0}{\partial y}, \tag{15}$$

$$(u_0, v_0) \cdot \mathbf{n} = 0, \quad \text{at the fixed boundary}, \tag{16}$$

$$\zeta_0 = \zeta_{\text{open}}, \quad x = 0. \tag{17}$$

In the above equations, $\mathbf{n}$ is the unit vector normal to the land boundary and ζ_{open} is the nondimensional water elevation at the open boundary.

According to Eq. 15, ζ_0 is a function of x and t but independent of y. This is an obvious inference caused by the narrow nature of the bay, which does not need to be an assumption as proposed in Li and O'Donnell (2005). According to Eqs. 14 and 15, the Coriolis force does not influence the zeroth-order tide. If the mean water depth is 10 m, $f = 10^{-4}\text{s}^{-1}$ and a semi-diurnal tide has a characteristic amplitude of 1 m, then $O(\delta) = O(B/FR) = O(B/100\text{km})$, where $R = \sqrt{gh_c}/f$ is the barotropic Rossby deformation radius. This means that B should be less than 10 km for the bay to be considered as a narrow one.

The equations for the first-order motions are

$$\frac{\partial \zeta_1}{\partial t} + \frac{\partial h u_1}{\partial x} + \frac{\partial h \upsilon_1}{\partial y} = -\left(\frac{\partial u_0 \zeta_0}{\partial x} + \frac{\partial \upsilon_0 \zeta_0}{\partial y}\right), \tag{18}$$

$$\frac{\partial u_1}{\partial t} - F\upsilon_0 = -\frac{\partial \zeta_1}{\partial x} - \beta_T \frac{u_1}{h} - \left(u_0 \frac{\partial u_0}{\partial x} + \upsilon_0 \frac{\partial u_0}{\partial y} - \beta_{T1} \frac{u_0 \zeta_0}{h^2}\right), \tag{19}$$

$$F u_0 = \frac{\partial \zeta_1}{\partial y}, \tag{20}$$

$$(u_1, \upsilon_1) \cdot \mathbf{n} = 0, \quad \text{at the fixed boundary}, \tag{21}$$

$$\zeta_1 = 0, \quad x = 0. \tag{22}$$

In the above equations, $\beta_{T1} = \beta_1 T/h_c$ with β_1 being equal to β. If β_1 is assumed to be 0, then the bottom friction term in Eqs. 11 and 12 retreats to the linear form case (see Feng et al. 1986a, Eqs. 3 and 4). This case is referred to as the "linear form of the bottom friction term" for short hereafter. Otherwise, it is called the "nonlinear form of the bottom friction term". The effect of these two forms on the residual current will be discussed in Section 4.4.

2.3 Equations for $\mathbf{u_L}$

In the present study, only a single frequency tide is imposed at the open boundary, i.e.,

$$\zeta_{\text{open}} = \zeta_{\text{open}R} \cos 2\pi t + \zeta_{\text{open}I} \sin 2\pi t = \text{Re}\left[\zeta^c_{\text{open}} e^{-i2\pi t}\right],$$

where $\zeta^c_{\text{open}} = \zeta_{\text{open}R} + i\zeta_{\text{open}I}$.

The solution of the zeroth-order tide takes the form of

$$\zeta_0 = \zeta_{0R} \cos 2\pi t + \zeta_{0I} \sin 2\pi t = \text{Re}\left[\zeta^c_0 e^{-i2\pi t}\right], \tag{23}$$

$$u_0 = u_{0R} \cos 2\pi t + u_{0I} \sin 2\pi t = \text{Re}\left[u^c_0 e^{-i2\pi t}\right], \tag{24}$$

$$\upsilon_0 = \upsilon_{0R} \cos 2\pi t + \upsilon_{0I} \sin 2\pi t = \text{Re}\left[\upsilon^c_0 e^{-i2\pi t}\right], \tag{25}$$

where $\zeta^c_0 = \zeta_{0R} + i\zeta_{0I}$, $u^c_0 = u_{0R} + iu_{0I}$ and $\upsilon^c_0 = \upsilon_{0R} + i\upsilon_{0I}$.

The nondimensional equivalence of Eq. 5 is

$$\langle f \rangle = \frac{1}{n} \int_{t_0}^{t_0+n} f(\mathbf{x}, t) \mathrm{d}t. \tag{26}$$

By applying the operator (Eq. 26) to Eqs. 18–20 and taking into consideration the forms of the zeroth- and first-order solutions in Feng et al. (1986a), the equations governing the first-order LRV for the weakly nonlinear tide can be obtained according to the methodology proposed by Feng (1987). The detailed procedure to obtain them is presented in the Appendix.

The equations governing the first-order LRV equations in a narrow bay are

$$\frac{\partial h u_L}{\partial x} + \frac{\partial h \upsilon_L}{\partial y} = 0, \tag{27}$$

$$u_L = \frac{h}{\beta_T}\left(-\frac{\partial \zeta_E}{\partial x} + \pi_x\right), \tag{28}$$

$$\frac{\partial \zeta_E}{\partial y} = 0, \tag{29}$$

where

$$\pi_x = \pi_{xN} + \pi_{x\beta}, \tag{30}$$

$$\pi_{xN} = -\frac{1}{2}\frac{\partial}{\partial x}\left\langle \xi_0 \frac{\partial \zeta_0}{\partial x} \right\rangle, \tag{31}$$

$$\pi_{x\beta} = \beta_{T1} \frac{\langle u_0 \zeta_0 \rangle}{h^2} + \frac{\beta_T}{h}\left(\frac{1}{h}\frac{\partial \langle h u_0 \eta_0 \rangle}{\partial y} + \langle \xi_0 \nabla \cdot \mathbf{u_0} \rangle + \left\langle -\eta_0 \frac{\partial u_0}{\partial y} \right\rangle\right), \tag{32}$$

$$\mathbf{u_L} \cdot \mathbf{n} = 0, \quad \text{at the fixed boundary}, \tag{33}$$

$$\zeta_E = 0, \quad x = 0. \tag{34}$$

Equation 28 tells that the longitudinal LRV can be obtained directly. The terms contributing to $\mathbf{u_L}$ include the gradient of the residual water elevation and a depth-averaged version of the tidal body force π_x, which was first defined by Feng (1987). The irrotational term π_{xN} represents the horizontal gradient of the tidally averaged coupling of the parcel displacement and the gradient of the water elevation. The rotational term $\pi_{x\beta}$ is more complex and is controlled by the bottom friction. It includes four terms corresponding to four mechanisms to drive the LRV. The first represents the tidally averaged interaction between the velocity and the water elevation. It diminishes when the tidal wave is a standing wave or when the tidal bottom friction term is in the linear form. The second is u_D defined in Eq. 8 and will be discussed in detail in Section 4.1. It is the gradient of the coupling of the water depth, the tidal current velocity in one direction and the water parcel displacement in the other direction. The third is the tidally averaged product of the along-channel water parcel displacement and the divergence of the velocity. The fourth is the tidally averaged product of the lateral water parcel displacement and the vorticity of the tidal current.

After the solution of the first-order LRV ($\mathbf{u_L}$) is obtained, the second-order LRV ($\mathbf{u_{ld}} = (u_{ld}, \upsilon_{ld})$) can be formulated as

$$u_{ld} = u'_{ld}\cos 2\pi t_0 + u''_{ld}\sin 2\pi t_0, \tag{35}$$

$$\upsilon_{ld} = \upsilon'_{ld}\cos 2\pi t_0 + \upsilon''_{ld}\sin 2\pi t_0, \tag{36}$$

$$u'_{ld} = u_{0I}\frac{\partial u_L}{\partial x} + \upsilon_{0I}\frac{\partial u_L}{\partial y} - u_L\frac{\partial u_{0I}}{\partial x} - \upsilon_L\frac{\partial u_{0I}}{\partial y}, \tag{37}$$

$$u''_{ld} = -u_{0R}\frac{\partial u_L}{\partial x} - \upsilon_{0R}\frac{\partial u_L}{\partial y} + u_L\frac{\partial u_{0R}}{\partial x} + \upsilon_L\frac{\partial u_{0R}}{\partial y}, \tag{38}$$

$$\upsilon'_{ld} = u_{0I}\frac{\partial \upsilon_L}{\partial x} + \upsilon_{0I}\frac{\partial \upsilon_L}{\partial y} - u_L\frac{\partial \upsilon_{0I}}{\partial x} - \upsilon_L\frac{\partial \upsilon_{0I}}{\partial y}, \tag{39}$$

$$\upsilon''_{ld} = -u_{0R}\frac{\partial \upsilon_L}{\partial x} - \upsilon_{0R}\frac{\partial \upsilon_L}{\partial y} + u_L\frac{\partial \upsilon_{0R}}{\partial x} + \upsilon_L\frac{\partial \upsilon_{0R}}{\partial y}. \tag{40}$$

3 Solutions in a narrow bay

For a rectangular bay, its constant width B can be taken as the length scale in y direction. Thus, $x = L_N$, $y = 0$ and $y = 1$ constitute the fixed boundary of the bay, where $L_N = L/\lambda$ is the dimensionless length of the bay which influences the solution together with β_T. The solution of Eqs. 13–17 for the zeroth-order tide in the above narrow bay is given in Li and Valle-Levinson (1999), but the assumption that the transverse gradient of the tidal elevation is zero in Li and Valle-Levinson (1999) is not needed here. According to Eq. 15, ζ_0 is independent of y, i.e., $\zeta_0 = \zeta_0(x, t)$, which is a natural deduction for a narrow bay system.

3.1 General solutions

If the water depth varies only along the bay, i.e., $h = h(x)$, then υ is always 0 according to Eqs. 13–17. For nonzero υ the water depth h should at least depend on y, the across-bay direction. Here, the case of $h = h(y)$ is considered.

The solution procedure of the linear tide follows Li and Valle-Levinson (1999) and the time invariant parts of the solution defined in Eqs. 23–25 are

$$\zeta_0^c(x) = \zeta_{\text{open}}^c\frac{\cos[\Omega(x - L_N)]}{\cos(\Omega L_N)}, \tag{41}$$

$$u_0^c(x, y) = -\zeta_{\text{open}}^c\frac{\Omega}{i2\pi - \beta_T/h}\frac{\sin[\Omega(x - L_N)]}{\cos(\Omega L_N)}, \tag{42}$$

$$\upsilon_0^c(x, y) = \frac{\zeta_{\text{open}}^c}{h}\frac{\cos[\Omega(x - L_N)]}{\cos(\Omega L_N)}\cdot \left[i2\pi y + \Omega^2\int_0^y \frac{h}{i2\pi - \beta_T/h}\mathrm{d}y'\right], \tag{43}$$

where

$$\Omega^2 = -\frac{i2\pi}{\mathcal{H}},$$

$$\mathcal{H} = \int_0^1 \left(\frac{h}{i2\pi - \beta_T/h}\right)\mathrm{d}y.$$

The first-order LRV is obtained in the following procedure. By applying the operator $\int_0^1 \mathrm{d}y$ to Eq. 27 with the boundary conditions taken into consideration, the following equation can be obtained,

$$\int_0^1 hu_L\mathrm{d}y = 0.$$

Then the substitution of Eq. 28 into the above relation followed by a rearrangement yields

$$\frac{\partial \zeta_E}{\partial x} = \frac{\int_0^1 h^2 \pi_x \mathrm{d}y}{\int_0^1 h^2 \mathrm{d}y}. \tag{44}$$

Thus, ζ_E can be obtained by integrating the above equation from 0 to x with $\zeta_E = 0$ at $x = 0$.

By substituting Eq. 44 into Eq. 28, one gets

$$u_L = \frac{h}{\beta_T \int_0^1 h^2 \mathrm{d}y} \left(\pi_x \int_0^1 h^2 \mathrm{d}y - \int_0^1 h^2 \pi_x \mathrm{d}y \right). \tag{45}$$

Then υ_L can be calculated by integrating Eq. 27 from 0 to y. Thus, the first-order LRV, $\mathbf{u_L}$, is expressed explicitly with the solution of the zeroth-order tide.

The Lagrangian drift velocity $\mathbf{u_{ld}}$ can be obtained with Eqs. 35–40 after the zeroth-order tidal current and the first-order LRV are obtained.

The explicit expression of each term in the solution is obtained by using Maxima, a system for the manipulation of symbolic and numerical expressions. It evolves from Macsyma, a computer algebra system developed in the late 1960s at Massachusetts Institute of Technology (Maxima.sourceforge.net 2009). The expression is exported as a segment of a Fortran code and inserted in a Fortran program directly. In the solution the integration concerning the water depth cannot always be solved analytically, so a numerical integration software package Quadpack is used (Piessens et al. 1983). To ensure accuracy, the double precision real number is used.

3.2 Solution for a specific bottom profile

The water depth across the bay is assumed to taken the dimensional form of

$$\widetilde{h}(y) = \widetilde{h}_1 + \widetilde{h}_2 e^{-[(y/B - 1/2)/\alpha]^2}, \tag{46}$$

where α is an adjusting parameter.

In the nondimensional form the bottom topography is

$$h(y) = h_1 + h_2 e^{-[(y-1/2)/\alpha]^2}, \tag{47}$$

where $h_1 = \widetilde{h}_1 / h_c$ and $h_2 = \widetilde{h}_2 / h_c$, The nondimensional form y is written the same as its dimensional counterpart for simplicity, as stated in Section 2.

Because the width of the bay, B, is neither in the depth profile nor in the residual circulation equations explicitly, the nondimensional results are independent of B if the narrow bay condition $O(\delta) \leq O(\kappa) < 1$ is satisfied.

The dimensional parameters in Eq. 46 are set the same as those in Li and O'Donnell (2005), with $\alpha = 7/40$ and the width $B = 2{,}000$ m. The water depth in the cross section of the bay (in meters) becomes

$$\widetilde{h}(y) = \widetilde{h}_1 + \widetilde{h}_2 e^{-[(y-2{,}000/2)/350]^2}.$$

If $\widetilde{h}_1 = 5$ m and $\widetilde{h}_2 = 10$ m, the nondimensional depth profile across the bay is displayed in Fig. 1.

A single-frequency tide with the period T =12 h is imposed with the amplitude of 1 m at the open boundary. The bottom friction coefficient is taken to be $\beta = \beta_1$ =0.00176 m s^{-1} as in Li and O'Donnell (2005). All the above parameters determine the nondimensional parameters in the narrow bay system (Eqs. 13–17 and 27–34), except the length of the bay. This configuration is referred to as the standard case in the remaining parts of the paper.

Based on the above configuration, the bay with a length $L = 105$ km is first considered. The Eulerian residual transport velocity $\mathbf{u_T}$ is displayed in Fig. 2 with the variables being in the nondimensional form. It can be seen that the flow pattern is symmetric with respect to the central line of the bay. Two mirror-symmetric gyres are formed at the head of the bay with the inward flow in the deep water area. At the outer part of the bay, two semi-gyres are formed with openings at the open boundary. The Eulerian residual transport velocity is outward at the deep water area and inward at the shoal area in the outer half of the bay. This result is consistent with that of Li and O'Donnell (2005).

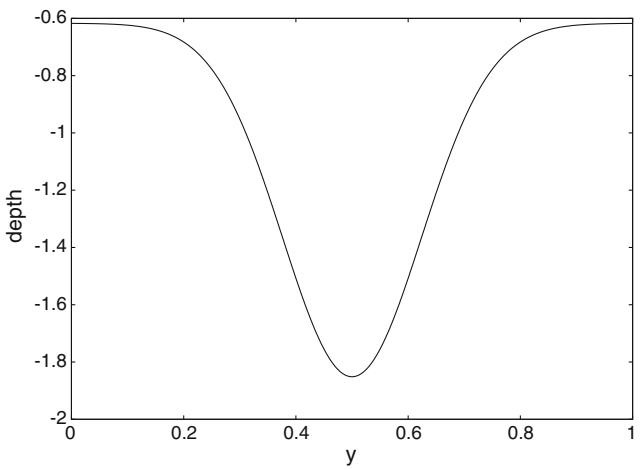

Fig. 1 The nondimensional depth profile across the bay

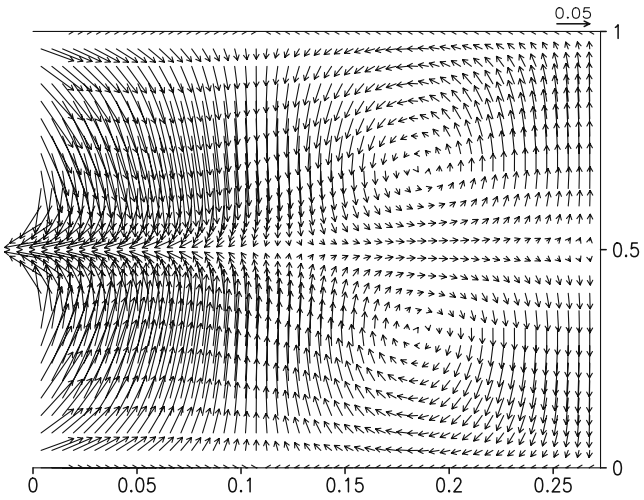

Fig. 2 The vectors of $\mathbf{u_T}$ in a bay of 105 km long and 2 km wide. All the labels and vectors are in the nondimensional form

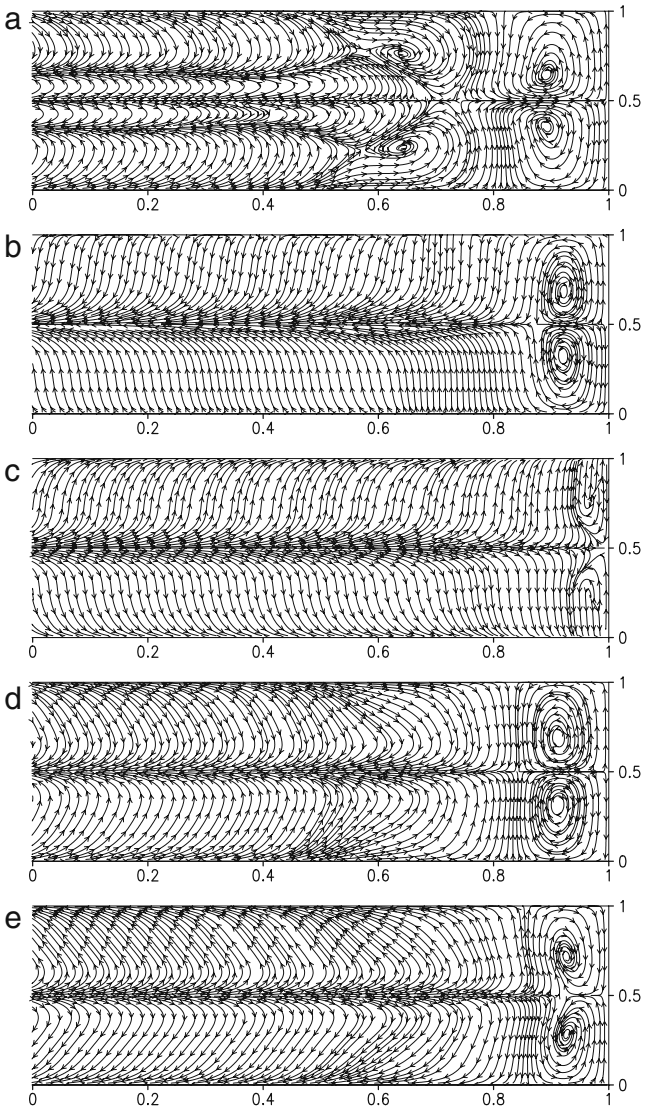

Fig. 3 Streamlines of nondimensional **a** $\mathbf{u_L}$, **b** $\mathbf{u_E}$, **c** $\mathbf{u_S}$, **d** $\mathbf{u_T}$, and **e** $\mathbf{u_D}$ in a bay with length equal to one tidal wavelength

4 Analysis of solutions in a narrow bay

4.1 $\mathbf{u_L}$ and its comparison with $\mathbf{u_E}$ and $\mathbf{u_T}$

The solutions of $\mathbf{u_L}$, $\mathbf{u_E}$, $\mathbf{u_S}$, $\mathbf{u_T}$ and $\mathbf{u_D}$ are displayed in Fig. 3 for the standard case with the length of the bay being the same as the tidal wave length.

The pattern of $\mathbf{u_L}$ shown in Fig. 3a is rather complex. A pair of mirror-symmetric gyres exist near the head of the bay, with the cyclonic one located in the upper half of the bay. Adjacent to these two gyres, there exists another pair of gyres with opposite rotation directions and they are compressed by four semi-gyres all extending to the open boundary. The four semi-gyres can be divided into two symmetric groups. In each group, the flow is inward along the lateral boundary and along the central axis of the bay; the two semi-gyres join together and flow out at the slope of the bay.

Distinct differences between $\mathbf{u_L}$ and $\mathbf{u_E}$ are found in the outer part of the bay. Figure 3b shows that the Eulerian residual velocity $\mathbf{u_E}$ flows outward along the whole open boundary, violating mass conservation law (Feng et al. 2008). However, Fig. 3c shows that $\mathbf{u_S}$ is in the opposite direction of $\mathbf{u_E}$ along the open boundary. As a result, the magnitude of $\mathbf{u_L}$, shown in Fig. 3a, has a smaller magnitude than that of $\mathbf{u_E}$ for the present case. This difference has been noticed in previous studies such as Loder (1980), but a more general theoretical explanation is given in this study. Figure 3b shows that there are two mirror-symmetric gyres near the head of the bay as in Fig. 3a, but the sizes of the gyres are different. The gyres of $\mathbf{u_L}$ occupy larger areas than those of $\mathbf{u_E}$.

$\mathbf{u_T}$ shown in Fig. 3d is different from $\mathbf{u_L}$ shown in Fig. 3a. Two semi-gyres, which are adjacent to the two gyres near the head of the bay, are located at the outer part. The two semi-gyres combine to form an outflow in the deep part of the bay and an inflow along the sides of the bay. At the open boundary $\mathbf{u_T}$ flows outward near the central axis of the bay while $\mathbf{u_L}$ flows inward; near the sides of the bay both $\mathbf{u_T}$ and $\mathbf{u_L}$ flow inward. For $\mathbf{u_L}$, we have noted that there exist two branches of outflows at the slope of the bay to ensure the mass conservation. Clearly, the LRV differs from the Eulerian residual transport velocity not only in magnitudes but also in patterns.

$\mathbf{u_D}$, the missing part in $\mathbf{u_T}$ for $\mathbf{u_L}$, is shown in Fig. 3e. Clearly, $\mathbf{u_D}$ countervails with $\mathbf{u_T}$ nearly everywhere.

This countervailing feature makes the magnitude of $\mathbf{u_L}$ smaller than $\mathbf{u_T}$; and even makes the directions of $\mathbf{u_L}$ and $\mathbf{u_T}$ opposite. This difference may suggest, for instance, that the "residence time of water inside the bay" estimated from $\mathbf{u_L}$ is longer than that estimated from $\mathbf{u_T}$.

$\mathbf{u_D}$ results from the interaction between the along-bay tidal velocity and the across-bay displacement, but the bottom topography still plays a role in determining it according to

$$u_D = \frac{\partial \ln h}{\partial y}\langle u_0\eta_0\rangle + \frac{\partial\langle u_0\eta_0\rangle}{\partial y}. \tag{48}$$

The tidally averaged product of the along-bay velocity and the across-bay displacement can be expressed as the product of u_0^c and the conjugate of v_0^c, v_0^{c*}, or the product of v_0^c and the conjugate of u_0^c, u_0^{c*}, i.e.,

$$\langle u_0\eta_0\rangle = -\langle v_0\xi_0\rangle = \frac{1}{4\pi}\mathrm{Im}\left(u_0^c v_0^{c*}\right) = -\frac{1}{4\pi}\mathrm{Im}\left(v_0^c u_0^{c*}\right). \tag{49}$$

Equation 49 is rather complex and Fig. 4 shows its distribution for a bay with length equal to 0.3 tidal wavelength since the major characteristics are confined to the head of the bay. The bay can be approximately split into four areas, with two bigger areas occupying the outer part of the bay and two smaller areas located near the head of the bay. $|\langle u_0\eta_0\rangle|$ is the biggest at the mouth of the bay and decreases towards the head of the bay. The variation of $\langle u_0\eta_0\rangle$ is also larger at the mouth than near the head of the bay. Across the outer part of the bay from $y = 0$ to $y = 1$, $\langle u_0\eta_0\rangle$ is negative for $y < 1/2$ and positive for $y > 1/2$. Meanwhile, $\partial \ln h/\partial y$ is positive in the lower half of the bay and negative in the upper half of the bay. Thus, the first term in Eq. 48 is negative across the bay. The second term in Eq. 48 is negative at the lateral boundary of the bay where the water is shallow, thus u_D is negative. u_D should be positive at the deep part of the bay because it obeys mass conservation. The condition is opposite near the head of the bay where two symmetric eddies exist. As a result, the pattern of $\mathbf{u_D}$ contrasts with that of $\mathbf{u_T}$ shown in Fig. 3d, e.

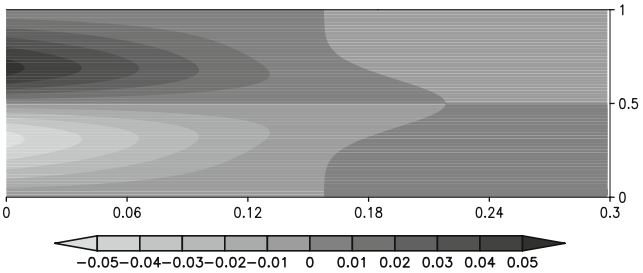

Fig. 4 The nondimensional form of $\langle u_0\eta_0\rangle$ in a narrow bay

4.2 Dependence on L_N

The nondimensional length of the bay, L_N, is a free parameter in the present case of a narrow bay. Here we examine the patterns of the first-order LRV by varying L_N from 0.12 to 0.5 tidal wavelength. Figure 5a shows that for the length of the bay being 0.5 wavelength, there are two mirror-symmetric gyres near the head of the bay as mentioned in Section 4.1 (Fig. 3a). The diameter of the gyres is about 0.18 wavelength. Again, in the outer part of the bay there are two gyres with different rotation directions, which are separated by four semi-gyres at the open boundary.

Figure 5b, c show the first-order LRV for the length of the bay being 0.3 and 0.12 wavelength respectively. The combination of Fig. 5 and Fig. 3a tells that the first-order LRV streamline of a shorter bay is a part of that of the longer bay. Therefore, the pattern of $\mathbf{u_L}$ is determined by the dimensionless distance away from the head of the bay, according to which the bay can be divided into three zones. In the inner zone, which is within 0.18 wave length away from the head of the bay, the water flows inward in the deep part and outward in the shallow part. In the outer zone, with distance larger than 0.5 wavelength, the water flows inward along the sides and in the deep part, and

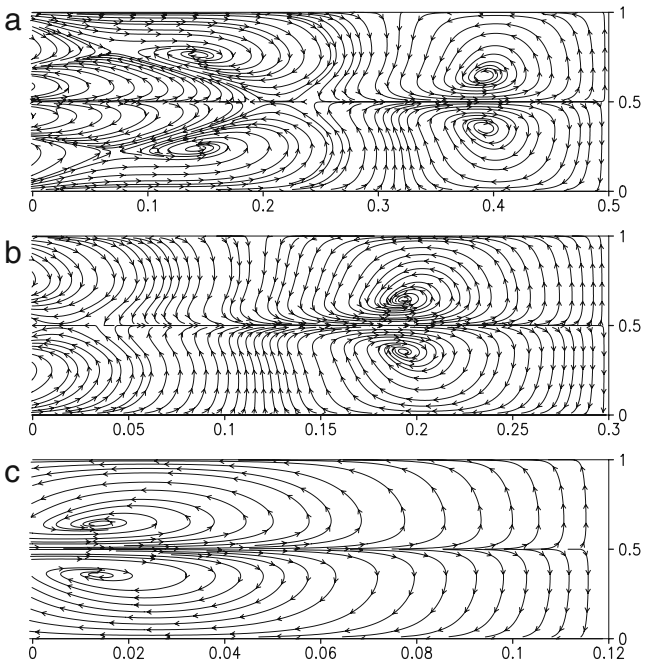

Fig. 5 The streamlines of nondimensional $\mathbf{u_L}$ in a bay with lengths of **a** 0.5, **b** 0.3, and **c** 0.12 tidal wavelength

flows outward in the slope area. The transition zone is located with distances between 0.18 and 0.5 wavelength away from the head of the bay. Here, the first-order LRV has a more complex pattern than the other two zones. The water flows inward along the sides and bounces back when encountering the two inner gyres; then the two branches will converge and flow outward for a short distance in the deep central part of the bay before detaching because of the inflow from the open boundary, and finally join together and flow outward in the slope area of the bay.

4.3 Dependence on β_T

According to Eq. 28, the nondimensional parameter $\beta_T = \beta T/h_c$ can influence the solution of LRV. Figures 6 and 7 show the streamlines of $\mathbf{u_L}$ and $\mathbf{u_T}$ with β_T being half or twice of that used for creating Fig. 3, respectively. With a reduced β_T, $\mathbf{u_L}$ is closer to $\mathbf{u_T}$ and the two semi-gyres located at the deep central part disappear. This corresponds to a reduced contribution of the rotational part of the tidal body force, $\pi_{x\beta}$. With an increased β_T, the gyres of $\mathbf{u_L}$ at the head of the bay do not appear but join the two semi-gyres in the deep central part of the bay. The structure of $\mathbf{u_T}$ does not change much with a changing β_T.

In the real world, the values of β_T differ for different bays with different water depths. For a single bay, the values of β_T differ for different tidal constitutes, for example, β_T for a semi-diurnal tide is only half of that for a diurnal tide. For a specific bay if the semi-diurnal and diurnal tides are both important, the residual current is induced by the combination of these tidal constituents. Under the weakly nonlinear condition, Feng (1990) proved that the Lagrangian residual current induced by multi-frequency tides is the linear summation of $\mathbf{u_L}$ generated by each tidal component. Therefore, the difference of the LRV caused by different values of β_T can add more complexity to the gross result than the single tide case. This suggests that the feature of the LRV may not be fully described by the bay length only.

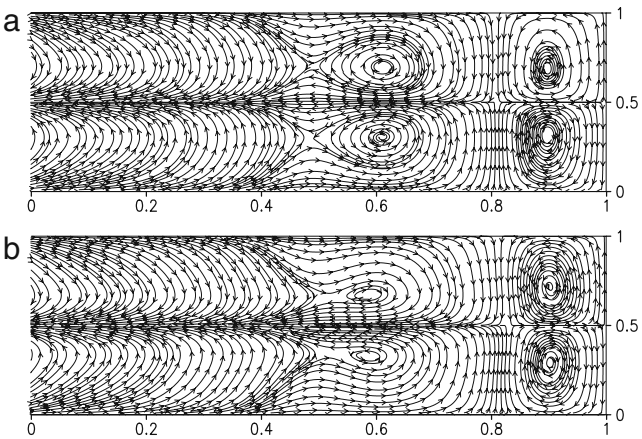

Fig. 6 The streamlines of nondimensional **a** $\mathbf{u_L}$ and **b** $\mathbf{u_T}$ with β_T being half of that used in creating Fig. 3

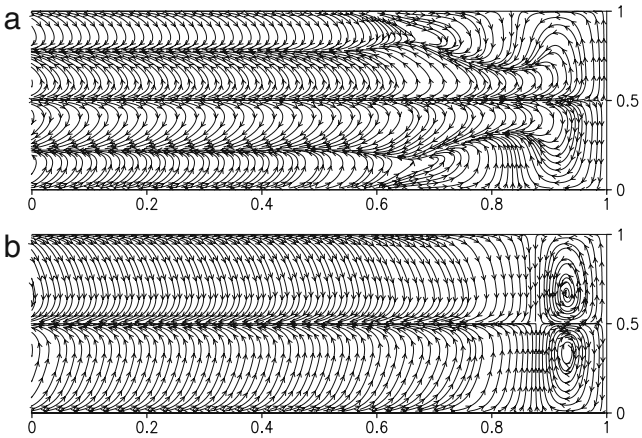

Fig. 7 The streamlines of nondimensional **a** $\mathbf{u_L}$ and **b** $\mathbf{u_T}$ with β_T being twice of that used in creating Fig. 3

4.4 Dependence on the form of the bottom friction

As stated in Section 2.2, the linearized bottom friction based on Proudman (1953) is used in this study. However, the bottom friction term in Eqs. 11 and 12 takes the nonlinear form, whereas in other studies the linear form, i.e., $\beta_{T1} = 0$, was used (Feng et al. 1986a).

It can be seen from Eqs. 13 to 15 that the zeroth-order tide is not influenced by the different forms of the bottom friction term. However, the nonlinear bottom friction term contributes to the first-order LRV through $\pi_{x\beta}$ in Eq. 28. The difference in $\mathbf{u_L}$ between the linear and nonlinear forms of the bottom friction is denoted as $\mathbf{u_{L\beta}} = (u_{L\beta}, v_{L\beta})$ and can be expressed as

$$u_{L\beta} = -\frac{h\int_0^1 \langle u_0\zeta_0\rangle \mathrm{d}y}{\beta_T \int_0^1 h^2 \mathrm{d}y} + \frac{\langle u_0\zeta_0\rangle}{\beta_T h}, \tag{50}$$

$$v_{L\beta} = \frac{\int_0^y h^2 \mathrm{d}y'}{\beta_T h \int_0^1 h^2 \mathrm{d}y} \int_0^1 \frac{\partial \langle u_0\zeta_0\rangle}{\partial x} \mathrm{d}y - \frac{1}{\beta_T h}\int_0^y \frac{\partial \langle u_0\zeta_0\rangle}{\partial x}\mathrm{d}y'. \tag{51}$$

The streamline of $\mathbf{u_L}$ for the linear form of the bottom friction term is shown in Fig. 8a. Compared with

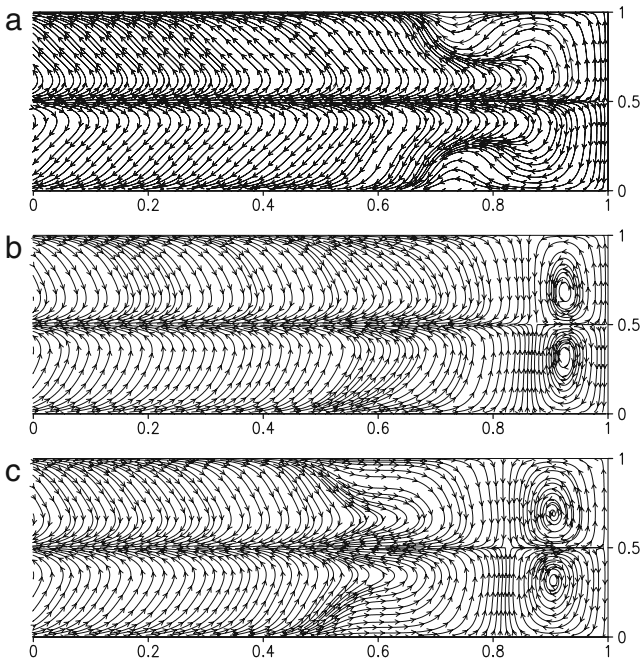

Fig. 8 **a** The streamline of $\mathbf{u_L}$ for linear bottom friction. **b** The streamline of $\mathbf{u_{L\beta}}$. **c** The streamline of $\mathbf{u_T}$ for linear bottom friction

Fig. 3a, it can be seen that the structure of $\mathbf{u_L}$ becomes much simpler. The two gyres near the head of the bay now disappear, and the four semi-gyres in the outer part of the bay are reduced to two semi-gyres with one occupying the upper and the other occupying the lower half of the bay.

The part of the LRV associated with the nonlinear part of the bottom friction term, $\mathbf{u_{L\beta}}$, is shown in Fig. 8b. Interestingly, the two gyres near the head of the bay in Fig. 8b are very similar to those in Fig. 3a. This means that the two gyres near the head of the bay in Fig. 3a are mainly induced by the nonlinear part of the bottom friction term. This explains why the pattern of $\mathbf{u_L}$ becomes two simple semi-gyres when the linear form of the bottom friction term is used. For the outer part, u_L in Fig. 8a is similar to u_D in Fig. 3e, both showing inward flow in the deep part and outward flow in the shallow shoal. If the nonlinear form of the bottom friction term is used, u_L becomes much more complex as displayed in Fig. 3a.

The pattern of $\mathbf{u_{L\beta}}$ shown in Fig. 8b is similar to that of $\mathbf{u_T}$ (Fig. 3d), but differs from that of $\mathbf{u_D}$ (Fig. 3e). Because $\mathbf{u_{L\beta}}$ is the difference in $\mathbf{u_T}$ between the cases using the linear and the nonlinear forms of the bottom friction, the structure of $\mathbf{u_T}$ for the linear form (Fig. 8c) does not show much difference with that of $\mathbf{u_T}$ for the nonlinear form of the bottom friction term (Fig. 3d). For the case of the linear form of the bottom friction term, the pattern of $\mathbf{u_T}$ differs from that of $\mathbf{u_L}$ in the outer part of the bay. $\mathbf{u_L}$ flows inward at the deep central part of the bay and flows outward in the shallow part and along the sides. $\mathbf{u_T}$ is in the opposite direction of $\mathbf{u_L}$. Despite of the above differences, $\mathbf{u_T}$ still shows two gyres near the head of the bay. This means that for the case of the linear form of the bottom friction term, the structure of the first-order LRV is smoother than that of the Eulerian residual transport velocity.

The bottom friction has two different effects on the residual current. In the case where the nonlinear form of the bottom friction term is used, only the nonlinear part associated with β_1 contributes to the generation of the residual velocity. The linear part associated with β only dissipates the residual current. In numerical modeling studies the bottom friction itself can be nonlinear, thus generating additional complexity.

4.5 Residual current and water exchange

One of the important applications of the residual transport is to estimate the water exchange. Many methods have been used to define the water exchange across a section. If the steady-state residual transport is obtained, the water volume bounded by a specific cross section divided by the water exchange flux at the same section is used to describe the residence time, denoted as "the residence time at that cross section" hereafter.

Since $h\mathbf{u_L}$ satisfies the mass conservation equation, the integration of hu_L over a section across the bay should be 0. The integration of $h|u_L|$ over half of the section across the bay is the water exchange flux at that section. The water exchange flux is calculated at the consecutive cross sections in a bay with a length of one tidal wavelength. The same procedure is also applied to $h|u_T|$. The resulting estimates are displayed in Fig. 9a.

It can be seen that the water exchange flux generally decreases from the open boundary towards the head of the bay; but at 0.18 wavelength away from the head of the bay, the water exchange flux reaches a minimum value. According to Fig. 3a, this is where the boundary of the two inner gyres is located. This location corresponds to a "barrier" for the water exchange in the bay. Similarly, Fig. 9b shows that the residence time increases sharply from the head of the bay and reaches the maximum at 0.18 wavelength away from the head. It then gradually decreases until toward the open boundary. Clearly, the variation of residence time along the bay corresponds to the two rather isolated circulation systems separated at 0.18 wavelength away from the head.

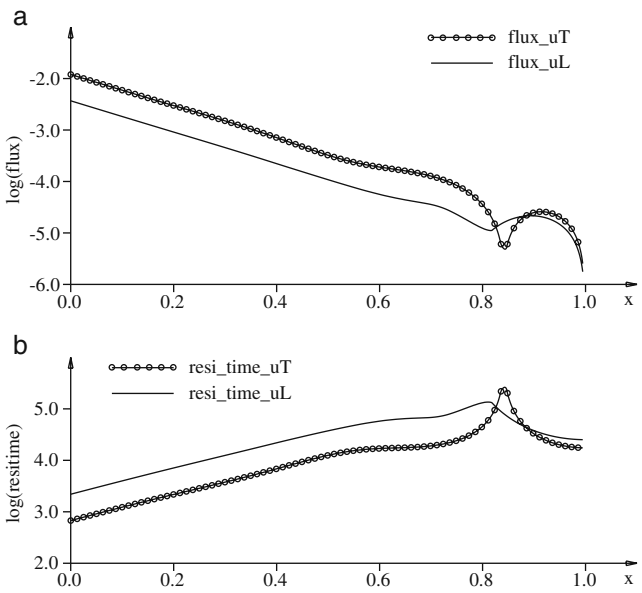

Fig. 9 **a** The water exchange flux at every cross section in a bay with length of one tidal wavelength based on hu_L and hu_T. **b** The residence time of water inside every cross section. The *vertical axes* are in logarithmic scales

The Eulerian residual transport, hu_T, is also used to estimate the water exchange and the resulting estimates are shown in Fig. 9a, b along with the estimates with the first-order Lagrangian residual transport hu_L. The characteristics of the estimates based on hu_T and hu_L are rather similar, but differ quantitatively. Firstly, the minimum water exchange flux based on hu_T occurs at around 0.16 wavelength away from the head, further inside the bay than that based on hu_L. This corresponds to the slight difference in the positions of the two gyres between the hu_L and hu_T cases. Secondly, the residence time based on hu_T is generally shorter than that based on hu_L, except near where the residence time reaches the maximum. At the open boundary, the residence time based on hu_L is three times longer than that based on hu_T. Therefore, if hu_T is used to examine the water exchange, the capacity of the physical self-purification of the bay will be significantly exaggerated.

The residence time for the bays with lengths ranging from 0.05 to 1 tidal wavelength is shown in Fig. 10. Clearly, the residence time increases with the length of the bay. The difference in the residence time between estimates based on hu_L and hu_T is nearly constant for the bays with lengths longer than 0.2 tidal wavelength.

The water exchange fluxes at each cross section for the bays with lengths ranging from 0.3 to 1 tidal wavelength are plotted in Fig. 11. By aligning the head of the bay at $x = 1$, the end of each curve line corresponds to the position of the open boundary. It can be seen

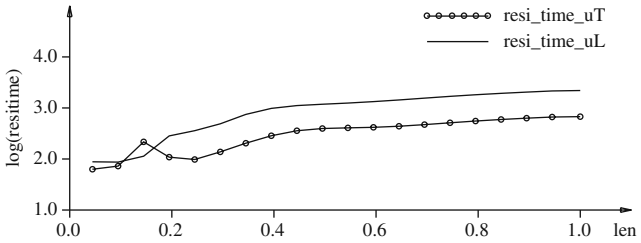

Fig. 10 The residence time based on hu_L and hu_T for the bays with different lengths. The *vertical axis* is in logarithmic scale

that the water exchange flux increases as the length of the bay decreases. For the same tidal energy input, the energy is spread further in a longer bay than in a shorter bay. At the open boundaries, the water exchange fluxes are similar; while the rates of variation along the axes of the bays are similar for the bays with various lengths. Interestingly, for bays with different lengths the minimum water exchange fluxes occur at the same location, i.e., at around 0.18 tidal wavelength away from the head of the bay, corresponding to the outer boundary of the two inner gyres.

The water exchange flux for a bay with different values of β_T is displayed in Fig. 12. The water exchange flux increases at most cross sections of the bay as β_T decreases. The minimum water exchange flux occurs where the inner and outer gyres are separated. That point is located at around 0.18 wavelength away from the head of the bay and shifts towards it as β_T increases. Moreover, the separation becomes less obvious as β_T gets bigger and finally the separation nearly disappears, corresponding to the merging of the inner and outer gyres as displayed in Fig. 7a.

The water exchange flux in bays with different depth profiles is examined by varying α from $2 \times 7/40$ to

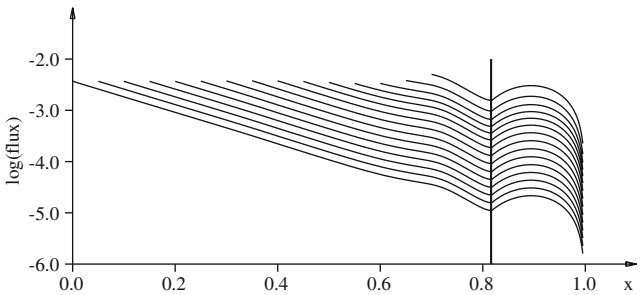

Fig. 11 The water exchange flux based on hu_L at each cross section of the bay with lengths ranging from 0.3 to 1 wave length, corresponding to *curves* displaced from *top* to *bottom*. The *vertical line* denotes the position where the minimum water exchange flux occurs. The *vertical axis* is in logarithmic scale

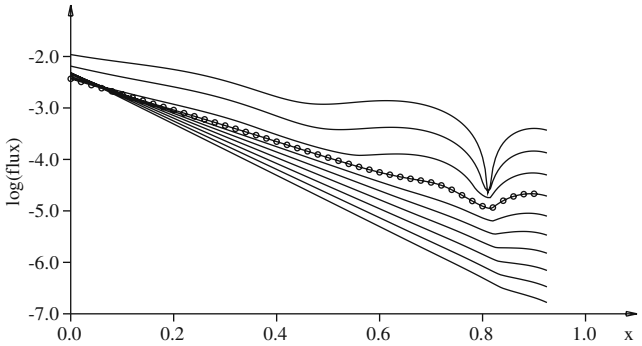

Fig. 12 The water exchange flux based on hu_L with different values of β_T, at each cross section of a bay with a length of one wave length. The *curves* from *top* to *bottom* correspond to the values of β_T being half and twice of that in the standard case. The *curve with circles* shows the standard case. The *vertical axis* is in logarithmic scale

$0.5 \times 7/40$ in Eq. 47 while keeping h_1 and h_2 unchanged. A constant is added to the depth profile to adjust the averaged water depth, so that β_T is kept the same as in the standard case. For $\alpha = 2 \times 7/40$, $1.4 \times 7/40$, and $1.0 \times 7/40$, the water exchange fluxes are displayed in Fig. 13. The results of $\alpha < 1 \times 7/40$ are not shown because they are very similar to that of $\alpha = 1 \times 7/40$. Figure 13 shows that the water exchange flux becomes bigger if α gets smaller, i.e., the bottom is flatter. The location of the minimum flux shifts away from the head of the bay when α gets bigger.

4.6 The second-order LRV

Equations 35 and 36 tell that the Lagrangian drift velocity depends on the initial tidal phase. At each location, the vectors of the Lagrangian drift velocity constitute an ellipse, as shown in Fig. 14. The ellipses are bigger

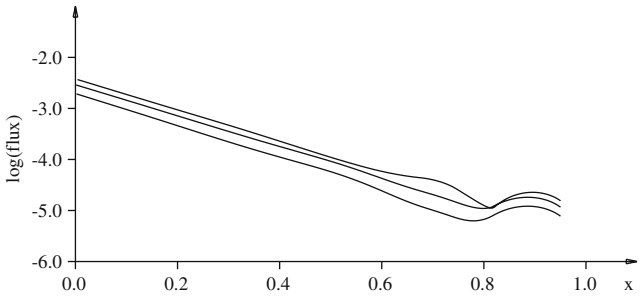

Fig. 13 The water exchange flux based on hu_L at each cross section of the bay with length of one wave length but different values of α. The *curves* from *bottom* to *top* correspond to $\alpha = 2 \times 7/40$, $1.4 \times 7/40$, and $1.0 \times 7/40$, respectively. The *vertical axis* is in the logarithmic scale

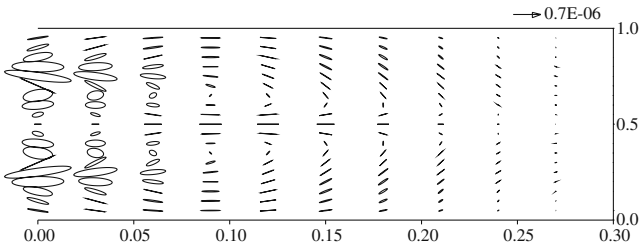

Fig. 14 Ellipses of the nondimensional $\mathbf{u_{ld}}$ in a narrow bay

at the open boundary and in the slope area of the bay. The ellipses are one order of magnitude smaller compared with the mass-transport velocity. Therefore, in this weakly nonlinear case the mass-transport velocity is a good approximation of the LRV. On the other hand, the dependence of the LRV on the initial tidal phase is a Lagrangian feature, which is important in many applications such as choosing the optimal time for sewage discharge.

5 Conclusions

In the present study, the depth-averaged equations for the single frequency tidal currents and the first-order LRV, and the expressions for the second-order LRV, are derived systematically based on the weakly nonlinear assumption. The equations are simplified for the case of a narrow bay and are solved analytically. The results for a specific axisymmetric bottom topography are discussed in detail.

Generally, according to the streamlines of the first-order LRV, the bay can be divided into an inner part near the head of the bay, the transitional zone, and the outer part near the open boundary. Two mirror-symmetric gyres exist in the inner part with the inflow in the central deep region. Adjacent to the two gyres in the inner part, two gyres with opposite rotation directions exist in the transitional zone. These two gyres are compressed by four semi-gyres in the outer part, where the water flows inward along the sides and the deepest part of the bay and flows outward along the slope.

The dependence of the first-order LRV on the length of the bay length, L_N, is examined. It is proved that the streamline of the nondimensional current velocity in a shorter bay is only part of that in a longer bay. The nondimensional parameter $\beta_T = \beta T/h_c$ includes the combined influences of the bottom friction parameter, the tidal period and the averaged water depth on the first-order LRV. For smaller values of β_T, the first-order LRV is closer to the Eulerian residual transport

velocity. For larger values of β_T, the two gyres in the inner part of the bay tend to merge with two of the four semi-gyres in the outer part. A practical significance in that the semi-diurnal or diurnal tides can change β_T by a factor of two. The form of the bottom friction also plays an important role in the pattern of the first-order LRV. This suggests that the parameterization of bottom friction in numerical models should be treated carefully.

The water exchange at each cross section of the bay is controlled by the LRV. The water exchange flux is higher at the open boundary and decreases towards the head of the bay, but the minimum flux occurs at around 0.18 wave length away from the head of the bay. This location can be regarded as where the inner and the outer parts of the bay separate. The position of this separation location is not fixed; it changes with both β_T and the bottom topography.

The second-order LRV is shown to be dependent on the initial tidal phase to take the Lagrangian averaging. This shows the Lagrangian feature of the LRV.

Different definitions of the residual current are different, not only in magnitudes but also in patterns and directions. The Eulerian residual transport velocity, that can be regarded as the partially modified Eulerian residual velocity, differs from the LRV. For the specific case considered here, the pattern of the Eulerian residual transport velocity is simpler than that of the first-order LRV; and in the deep part of the bay, the two velocities are in opposite directions. This leads to significant difference in the water residence time calculated according to different residual currents.

It is noteworthy that the symmetry of the depth profile about $y = 0.5$ is not a prerequisite to get the solution. Indeed there is a streamline along $y = 0.5$ so the narrow bay can be split into two separate bays without affecting the solutions. Thus, the depth profile can be of any form if it only varies in the across-bay direction.

In general the LRV represents the water mass intertidal transport in the tide dominant area. The residual current derived by other methods may cause the misunderstanding of the mass-transport mechanism in the study area. Yet, this belief is not easy to be proved in the field because in most tide dominant areas the residual current, which is of the order of cm s^{-1}, is a small part of the current. This value is even beyond the precision of the current meter. The traditional Eulerian observation cannot obtain the LRV, which makes the proof more difficult.

In this paper the depth-averaged LRV obtained analytically in the narrow bay gives a good example. Although it is confined to a single-frequency tidal case, the analysis can be extended to cases with wind driven, baroclinic, and multi-frequency tides, because the residual currents generated by the above factors can be linearly combined following Feng (1987, 1990). River runoff can also be included at the head of the bay based on the analyses of Feng and Wu (1995) and Feng (1998). Further steps to verify these theoretical analyses include laboratory experiments and the development of innovative methods of Lagrangian observations.

Acknowledgements This study was supported by project 40976003 from National Science Foundation of China and National Basic Research Program of China (2010CB428904). We thank the two anonymous reviewers for constructive comments on the original manuscript.

Appendix: The derivation of equations for $\mathbf{u_L}$

By applying the operator (Eq. 26) to Eq. 18 and making use of the definition of $\mathbf{u_E}$ in Eq. 3, one gets

$$\frac{\partial h u_E}{\partial x} + \frac{\partial h \upsilon_E}{\partial y} = -\left(\frac{\partial \langle u_0 \zeta_0 \rangle}{\partial x} + \frac{\partial \langle \upsilon_0 \zeta_0 \rangle}{\partial y}\right). \tag{52}$$

The substitution of Eqs. 23–25 into Eq. 4 gives

$$h u_S = \langle u_0 \zeta_0 \rangle + \frac{\partial}{\partial y} \langle h u_0 \eta_0 \rangle, \tag{53}$$

$$h \upsilon_S = \langle \upsilon_0 \zeta_0 \rangle + \frac{\partial}{\partial x} \langle h \upsilon_0 \xi_0 \rangle. \tag{54}$$

By performing $\partial/\partial x$ (Eq. 53) + $\partial/\partial y$ (Eq. 54) and taking into consideration of Eq. 52, the continuity equation of $\mathbf{u_L}$, Eq. 27, can be obtained.

The momentum equations of the LRV are derived as follows. By applying Eq. 26 to Eq. 19 and making use of Eq. 2, one gets

$$0 = -\frac{\partial \zeta_E}{\partial x} - \beta_T \frac{u_L}{h} + \beta_{T1} \frac{\langle u_0 \zeta_0 \rangle}{h^2} - \left\langle u_0 \frac{\partial u_0}{\partial x} + \upsilon_0 \frac{\partial u_0}{\partial y} \right\rangle + \beta_T \frac{1}{h} \left\langle \xi_0 \frac{\partial u_0}{\partial x} + \eta_0 \frac{\partial u_0}{\partial y} \right\rangle. \tag{55}$$

By applying the operator $(\xi_0 \partial/\partial x + \eta_0 \partial/\partial y)$ to Eq. 14 and making use of Eq. 15, followed by applying Eq. 26, one yields

$$\left\langle \xi_0 \frac{\partial^2 u_0}{\partial x \partial t} + \eta_0 \frac{\partial^2 u_0}{\partial y \partial t} \right\rangle = -\left\langle \xi_0 \frac{\partial^2 \zeta_0}{\partial x^2} \right\rangle - \beta_T \left\langle \xi_0 \frac{\partial}{\partial x}\left(\frac{u_0}{h}\right) + \eta_0 \frac{\partial}{\partial y}\left(\frac{u_0}{h}\right) \right\rangle. \tag{56}$$

The left side of Eq. 56 is rearranged with integration by parts. Furthermore, by making use of Eq. 6 and the periodicity of the variables, one gets

$$\left\langle \xi_0 \frac{\partial^2 u_0}{\partial x \partial t} + \eta_0 \frac{\partial^2 u_0}{\partial y \partial t} \right\rangle = \left\langle \frac{\partial}{\partial t}\left(\xi_0 \frac{\partial u_0}{\partial x} + \eta_0 \frac{\partial u_0}{\partial y} \right) \right\rangle - \left\langle \frac{\partial \xi_0}{\partial t}\frac{\partial u_0}{\partial x} + \frac{\partial \eta_0}{\partial t}\frac{\partial u_0}{\partial y} \right\rangle = -\left\langle u_0 \frac{\partial u_0}{\partial x} + \upsilon_0 \frac{\partial u_0}{\partial y} \right\rangle. \quad (57)$$

Then by changing Eq. 56 to the following form

$$-\left\langle u_0 \frac{\partial u_0}{\partial x} + \upsilon_0 \frac{\partial \upsilon_0}{\partial y} \right\rangle = -\left\langle \xi_0 \frac{\partial^2 \zeta_0}{\partial x^2} \right\rangle - \beta_T \frac{1}{h}\left\langle \xi_0 \frac{\partial u_0}{\partial x} + \eta_0 \frac{\partial u_0}{\partial y} \right\rangle - \beta_T \left\langle \xi_0 u_0 \frac{\partial}{\partial x}\left(\frac{1}{h}\right) + \eta_0 u_0 \frac{\partial}{\partial y}\left(\frac{1}{h}\right) \right\rangle,$$

and by adding Eq. 55 to the above equation, one gets

$$0 = -\frac{\partial \zeta_E}{\partial x} - \beta_T \frac{u_L}{h} + \beta_{T1} \frac{\langle u_0 \zeta_0 \rangle}{h^2} - \left\langle \xi_0 \frac{\partial^2 \zeta_0}{\partial x^2} \right\rangle - \beta_T \left\langle \xi_0 u_0 \frac{\partial}{\partial x}\left(\frac{1}{h}\right) + \eta_0 u_0 \frac{\partial}{\partial y}\left(\frac{1}{h}\right) \right\rangle. \quad (58)$$

By applying $\xi_0 \partial/\partial x$ to Eq. 14, one obtains

$$\xi_0 \frac{\partial^2 \zeta_0}{\partial x^2} = -\xi_0 \left(\frac{\partial^2 u_0}{\partial x \partial t} + \beta_T \frac{\partial}{\partial x}\left(\frac{u_0}{h}\right) \right), \quad (59)$$

and then $\partial/\partial x \left[\xi_0 \cdot (\text{Eq. } 14)\right]$ leads to

$$\frac{\partial}{\partial x}\left(\xi_0 \frac{\partial \zeta_0}{\partial x} \right) = -\frac{\partial}{\partial x}\left(\xi_0 \frac{\partial u_0}{\partial t} + \beta_T \xi_0 \frac{u_0}{h} \right). \quad (60)$$

Then, Eq. 59 is multiplied with 2 and subtracted with Eq. 60; and the resulting equation is averaged over one tidal period. By making use of Eq. 6 and the periodicity of the zeroth-order solution, one obtains

$$\left\langle \xi_0 \frac{\partial^2 \zeta_0}{\partial x^2} \right\rangle = \left\langle \frac{1}{2}\frac{\partial}{\partial x}\left(\xi_0 \frac{\partial \zeta_0}{\partial x} \right) \right\rangle + \beta_T \frac{1}{h}\left\langle u_0 \frac{\partial \xi_0}{\partial x} \right\rangle. \quad (61)$$

Substituting Eq. 61 into Eq. 58 leads to

$$0 = -\frac{\partial \zeta_E}{\partial x} - \beta_T \frac{u_L}{h} + \beta_{T1} \frac{\langle u_0 \zeta_0 \rangle}{h^2} - \left\langle \frac{1}{2}\frac{\partial}{\partial x}\left(\xi_0 \frac{\partial \zeta_0}{\partial x} \right) \right\rangle - \beta_T \left\langle \xi_0 u_0 \frac{\partial}{\partial x}\left(\frac{1}{h}\right) + \eta_0 u_0 \frac{\partial}{\partial y}\left(\frac{1}{h}\right) \right\rangle - \beta_T \frac{1}{h}\left\langle u_0 \frac{\partial \xi_0}{\partial x} \right\rangle. \quad (62)$$

For the case of single tidal frequency $\langle \xi_0 u_0 \rangle = \langle \eta_0 \upsilon_0 \rangle = 0$, thus

$$-\beta_T \left\langle \xi_0 u_0 \frac{\partial}{\partial x}\left(\frac{1}{h}\right) + \eta_0 u_0 \frac{\partial}{\partial y}\left(\frac{1}{h}\right) \right\rangle = \beta_T \frac{1}{h^2}\frac{\partial}{\partial y}\langle h u_0 \eta_0 \rangle + \beta_T \frac{1}{h}\left\langle \xi_0 \frac{\partial \upsilon_0}{\partial y} - \eta_0 \frac{\partial u_0}{\partial y} \right\rangle,$$

$$-\beta_T \frac{1}{h}\left\langle u_0 \frac{\partial \xi_0}{\partial x} \right\rangle = \beta_T \frac{1}{h}\left\langle \xi_0 \frac{\partial u_0}{\partial x} \right\rangle.$$

By applying the above results to Eq. 62, Eq. 28 can be obtained. It is trivial to obtain the momentum equation in the y direction.

References

Abbott MR (1960) Boundary layer effects in estuaries. J Mar Res 18:83–100

Cerco CF, Cole T (1993) Three-dimensional eutrophication model of Chesapeake Bay. J Environ Eng 119:1106–1125

Cheng RT (1983) Euler-Lagrangian computations in estuarine hydrodynamics. In: Taylor J, Johnson A, Smith R (eds) Proceedings of third international conference on numerical methods in laminar and turbulent flow. Pineridge, Swansea. pp 341–352

Cheng RT, Casulli V (1982) On Lagrangian residual currents with applications in South San Francisco Bay, California. Water Resour Res 18:1652–1662

Delhez EJM (1996) On the residual advection of passive constituents. J Mar Syst 8:147–169

Dortch MS, Chapman RS, Abt SR (1992) Application of three-dimensional Lagrangian residual transport. J Hydraul Eng 118:831–848

Dyke PPG (1980) On the Stokes' drift induced by tidal motions in a wide estuary. Estuarine Coastal Mar Sci 11:17–25

Feng S (1987) A three-dimensional weakly nonlinear model of tide-induced Lagrangian residual current and mass-transport, with an application to the Bohai Sea. In: Nihoul JCJ, Jamart BM (eds) Three-dimensional models of marine and estuarine dynamics, Elsevier Oceanography Series, 45. Elsevier, Amsterdam. pp 471–488

Feng S (1990) On the Lagrangian residual velocity and the mass-transport in a multi-frequency oscillatory system. In: Cheng RT (ed) Residual currents and long-term transport, Coastal and Estuarine Studies 38. Springer, Berlin, pp 34–48

Feng S (1998) On circulation in Bohai Sea Yellow Sea and East China Sea. In: Hong GH, Zhang J, Park BK (eds) Health of the Yellow Sea. The Earth Love Publication Association, Seoul, pp 43–77

Feng S, Wu D (1995) An inter-tidal transport equation coupled with turbulent K-ϵ model in a tidal and quasi-steady current system. Chin Sci Bull 40:136–139

Feng S, Xi P, Zhang S (1984) The baroclinic residual circulation in shallow seas. Chin J Oceanol Limnol 2:49–60

Feng S, Cheng RT, Xi P (1986a) On tide-induced Lagrangian residual current and residual transport, 1. Lagrangian residual current. Water Resour Res 22:1623–1634

Feng S, Cheng RT, Xi P (1986b) On tide-induced Lagrangian residual current and residual transport, 2. residual transport

with application in South San Francisco Bay. Water Resour Res 22:1635–1646
Feng SZ, Ju L, Jiang WS (2008) A Lagrangian mean theory on coastal sea circulation with inter-tidal transports, I. fundamentals. Acta Oceanol Sin 27:1–16
Fischer HB, List EJ, Koh R, Imberger J, Brooks NH (1979) Mixing in inland and coastal waters. Academic, New York
Foreman MGG, Baptista AM, Walters RA (1992) Tidal model studies of particle trajectories around a shallow coastal bank. Atmos Ocean 30:43–69
Hainbucher D, Wei H, Pohlmann T, Sündermann J, Feng S (2004) Variability of the Bohai Sea circulation based on model calculations. J Mar Syst 44:153–174
Hunt JN (1961) Oscillations in a viscous liquid with an application to tidal motion. Tellus 13:79–84
Ianniello JP (1977) Tidally induced residual currents in estuaries of constant breadth and depth. J Mar Res 35:755–786
Jay DA (1991) Estuarine salt conservation: a Lagrangian approach. Estuarine, Coastal Shelf Sci 32:547–565
Li C, O'Donnell J (2005) The effect of channel length on the residual circulation in tidally dominated channels. J Phys Oceanogr 35:1826–1840
Li C, Valle-Levinson A (1999) A two-dimensional analytic tidal model for a narrow estuary of arbitrary lateral depth variation: the intratidal motion. J Geophys Res 104:23,525–23,543
Li C, Chen C, Guadagnoli D, Georgiou IY (2008) Geometry-induced residual eddies in estuaries with curved channels: observations and modeling studies. J Geophys Res 113:C01,005. doi:10.1029/2006JC004031
Loder JW (1980) Topographic rectification of tidal currents on the sides of Georges Bank. J Phys Oceanogr 10:1399–1416
Longuet-Higgins MS (1969) On the transport of mass by time-varying ocean currents. Deep-Sea Res 16:431–447
Maxima.sourceforge.net (2009) Maxima, a computer algebra system version 5.18.1. Available at: http://maxima.sourceforge.net. Accessed 14 July 2010
Muller H, Blanke B, Dumas F, Lekien F, Mariette V (2009) Estimating the Lagrangian residual circulation in the Iroise sea. J Mar Syst 78:S17–S36. doi:10.1016/j.jmarsys.2009.01.008
Nihoul ICJ, Ronday FC (1975) The influence of the tidal stress on the residual circulation. Tellus A 27:484–489
Piessens R, de Doncker-Kapenga E, Überhuber C, Kahaner D (1983) Quadpack: a subroutine package for automatic integration, springer series in computational mathematics, vol 1. Springer, Berlin
Proudman J (1953) Dynamical oceanography. Methuen, London
Ridderinkhof H, Loder JW (1994) Lagrangian characterization of circulation over submarine banks with application to the outer Gulf of Maine. J Phys Oceanogr 24:1184–1200
Robinson IS (1983) Tidally induced residual flows. In: Johns B (ed) Physical oceanography of coastal and shelf seas. Elsevier, Amsterdam, pp 321–356
Wang H, Su Z, Feng S, Sun W (1993) A three dimensional numerical calculation of the wind driven thermohaline and tide-induced Lagrangian residual current in the Bohai Sea. Acta Oceanol Sin 12:169–182
Wei H, Hainbucher D, Pohlmann T, Feng S, Sündermann J (2004) Tidal-induced Lagrangian and Eulerian mean circulation in the Bohai Sea. J Mar Syst 44:141–151
Winant CD (2007) Three-dimensional tidal flow in an elongated, rotating basin. J Phys Oceanogr 37:2345–2362
Winant CD (2008) Three-dimensional residual tidal circulation in an elongated, rotating basin. J Phys Oceanogr 38:1278–1295
Zimmerman JTF (1979) On the Euler-Lagrange transformation and the Stokes' drift in the presence of oscillatory and residual currents. Deep-Sea Res 26A:505–520